NASA

Technical Memorandum 79580

A Three-Dimensional Model of Corotating Streams in the Solar Wind I. Theoretical Foundations

V. Pizzo

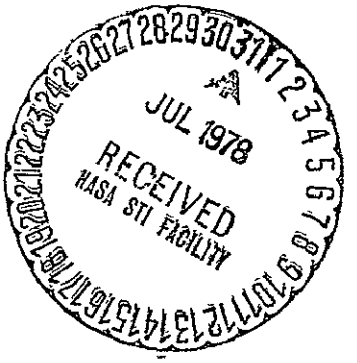

JUNE 1978

National Aeronautics and
Space Administration

Goddard Space Flight Center
Greenbelt, Maryland 20771

A THREE-DIMENSIONAL MODEL OF COROTATING STREAMS IN THE SOLAR WIND

I. THEORETICAL FOUNDATIONS

by

V. Pizzo*
NASA/Goddard Space Flight Center
Laboratory for Extraterrestrial Physics
Greenbelt, MD 20771

SUBMITTED TO: Journal of Geophysical Research

*NAS/NRC Resident Research Associate

ABSTRACT

This paper is concerned with the development of the theoretical and mathematical background pertinent to the study of steady, corotating solar wind structure in all three spatial dimensions (3-D). The dynamical evolution of the plasma in interplanetary space (defined as the region beyond roughly 35 $R_\odot$ where the flow is supersonic) is approximately described by the nonlinear, single-fluid, polytropic (magneto-) hydrodynamic equations. We outline efficient numerical techniques for solving this complex system of coupled, hyperbolic partial differential equations. The present formulation is inviscid and non-magnetic, but our methods allow for the potential inclusion of both features with only modest modifications. We examine one simple, highly idealized, hydrodynamic model stream to illustrate the fundamental processes involved in the 3-D dynamics of stream evolution. We find that spatial variations in the rotational stream interaction mechanism produce small nonradial flows on a global scale that lead to the transport of mass, energy, and momentum away from regions of relative compression and into regions of relative rarefaction. The magnitude of this transport is small, but inside 1 AU the nonradial flow can significantly retard shock formation by allowing fluid in the compressions to slip laterally, thereby partially relieving the stresses built up in the stream interaction. Comparison with simpler models demonstrates the essential nonlinear, multi-dimensional nature of the interplanetary dynamics. A subsequent paper will be devoted to the investigation of a wide range of more realistic model streams.

INTRODUCTION

The solar corona is frequently dominated by long-lived structures which are organized on a global scale. Since the solar wind has its origin in the coronal expansion, it is natural to expect that the large-scale flow pattern of the solar wind reflect the three-dimensional (3-D) structure of the corona (for a recent review covering the relationship between coronal structure and the solar wind, see Hundhausen, 1977). Indeed, inferences drawn from a variety of spacecraft and interplanetary-scintillation observations provide compelling evidence that much of this structure survives to the earth and beyond (e.g., see Dobrowolny and Moreno, 1976).

One important class of solar wind flow is the stream interaction (or "colliding streams"), which refers to the dynamical process by which steady, large-scale inhomogeneities in the coronal expansion speed couple with solar rotation to produce significant longitudinal rearrangement of material in interplanetary space. The basic mechanism is illustrated in Figure 1, where we view the flow in the ecliptic plane from above the north pole of the sun. The fast material emanating radially from the high-speed source region near the sun is subsequently aligned by solar rotation with the preceding slower plasma, resulting in a spiral interaction structure at large heliocentric distances. Material piles up at the leading edge of the stream, where the fast flow overtakes the slow, while material in the trailing portions of the stream is rarefied. Nonradial motions (aside from those impressed upon the flow at the source) are driven by the lateral pressure gradients associated with

the compression along the interaction front. But note that the rotation introduces a basic anisotropy into the picture: the azimuthal gradients are directly driven by the stream interaction mechanism, while the meridional gradients (out of the plane of the paper) arise as a consequence of latitudinal variations in that mechanism. The latitudinal variation stems partly from intrinsic latitudinal variations in the corona and partly from the latitudinal dependence of the rotational effect. That is, for structures of the same spatial width, those lying nearer the equator suffer a greater rotational interaction than those lying nearer the poles. In general, therefore, we expect the meridional gradients, and, hence, meridional motions, to be somewhat different from their azimuthal counterparts.

Theoretical interest in the corotating stream interaction has centered on the description of the mechanism in the neighborhood of the solar equatorial plane, giving rise to increasingly complex 2-D models whose validity depends upon the absence or negligibility of the local latitudinal gradients, i.e., 3-D structure. Practical computational difficulties have hindered progress toward 3-D formulations of comparable sophistication. The 3-D linear model (Siscoe and Finley, 1972) proves inadequate in the face of the large-amplitude variations in streams, while the kinematic description (Barouch and Burlaga, 1976) neglects the dynamical reaction of the plasma. A nonlinear 3-D approximation has been synthesized under the assumption of purely radial flow (Suess et al., 1975), but the effects of the nonradial motions are not taken into account. Axisymmetric models (e.g., Siscoe and Finley, 1969; Suess, 1972; Nerney and Suess, 1975) include the meriodional flow but ignore the essential azimuthal properties of the stream interaction.

A nonlinear 3-D stream model could provide valuable insights on both observational and theoretical fronts. For example, spacecraft observations of the interplanetary medium are confined to a narrow zone about the ecliptic plane. Lest our interpretation of these data become ensnared in the parochial viewpoint imposed by our limited sampling capabilities, it is imperative that we acquire the requisite expertise to treat these observations in context, i.e., as nothing other than the ecliptic manifestation of a phenomenon that is fundamentally global in nature. Likewise, the analysis of interplanetary scintillation and radio scattering observations, which contribute useful but less detailed information on high-latitude and near-sun flows, would benefit from the availability of a more complete description of the overall solar wind flow structure. As a matter of theoretical interest, the strengths and weaknesses of established but less elaborate models could be evaluated and the inferences drawn from them more knowledgeably assessed. Finally, we could take advantage of the capabilities of a sophisticated 3-D model to speculate upon the properties of the solar wind flow in regions currently inaccessible to empirical study.

In this paper, we develop a fully nonlinear 3-D model of steady corotating streams in the solar wind. The treatment is hydrodynamic, polytropic, and inviscid, and describes the flow in the supersonic regime (beyond $\sim 35\ R_\odot$). We outline mathematical and computational techniques that form the basis for a family of stream models that will eventually

be extended to a nonlinear, 3-D MHD formulation. We consider here one simple example intended to facilitate the conceptualization of 3-D stream dynamics, contrasting the properties of our global solutions with those of simpler models that have appeared in the literature. A subsequent paper will be devoted to the examination of a number of more complex and realistic cases, which are better suited to physical generalization.

MATHEMATICAL DESCRIPTION OF THE FLOW

Numerous published models dealing with the dynamics of corotating high-speed streams (e.g., Siscoe and Finley, 1972; Matsuda and Sakurai, 1972; Goldstein, 1971, Hundhausen, 1973; Nakagawa and Wellck, 1974; Dryer and Steinolfsson, 1976; and Goldstein and Jokipii, 1977) have been based upon the magnetohydrodynamic (MHD) description of the solar wind flow first espoused by Parker (1958). It can be shown that the kinetic equations reduce to the MHD formulation on the condition that we restrict attention to structures that are much larger than the standard plasma scale lengths (e.g., gyration radius, Debye length, etc.) and to regions some distance from the sun ($r \gtrsim 35\ R_\odot$) where the flow is supersonic and the dynamics dominated by rotation and inertia (Pizzo, 1977). It is presumed that the solar wind can be treated as a neutral electron-proton gas having infinite electrical conductivity, and that heat conduction, viscosity, and small-scale wave phenomena may be neglected. Furthermore, the magnetic field may be dropped from the formulation on the grounds that the flow is heavily momentum-dominated and magnetic effects therefore minor. This assertion is justified for the relatively broad structures we will consider here, but may break down at large radial distances ($r > 1$ AU) where the streams approach shock formation or much nearer the sun in the case of streams having initially sharp boundaries (Rosenbauer *et al.*, 1977; Gosling *et al.*; 1978; Pizzo and Burlaga, 1977).

The 3-D HD equations for the corotating solar wind flow are, in vector form in the inertial (nonrotating) frame:

$$-\Omega \frac{\partial \rho}{\partial \phi} + \nabla \cdot \rho \vec{U} = 0 \tag{1a}$$

$$-\Omega \frac{\partial \vec{U}}{\partial \phi} + (\vec{U} \cdot \nabla)\vec{U} = -\frac{1}{\rho} \nabla p - \frac{GM_\odot}{r^2} \hat{r} \tag{1b}$$

$$\left(-\Omega \frac{\partial}{\partial \phi} + \vec{U} \cdot \nabla\right) P \rho^{-\gamma} = 0 \tag{1c}$$

where ρ is the (proton) mass density, $\vec{U}$ the center-of-mass velocity, P the total isotropic gas pressure, G the gravitational constant, $M_\odot$ the solar mass, and γ the polytropic index. The independent variables are the usual spherical-polar coordinates (r, θ, ϕ), and the parameter Ω is the equatorial angular rotation rate of the sun (differential rotation is neglected). These three equations express the conservation of mass, momentum, and polytropic constant respectively.

We set $\gamma = 5/3$, the adiabatic value, to minimize the number of free parameters in the calculation (that is, temperature changes in the plasma are determined entirely by the work performed in compressions and rarefactions). This choice does force the use of somewhat elevated temperatures near the sun if one is to match average solar wind conditions near the earth, leading to an overall radial acceleration between the inner boundary and 1.0 AU. However, these effects do not seriously affect our results, and we would rather deal with these complications than with the physical ambiguities introduced by a non-adiabatic γ. Finally, the first term in each of equations (1) arises from the relation between temporal and azimuthal gradients for corotating structure in the inertial frame,

$$\frac{\partial}{\partial t} = -\Omega \frac{\partial}{\partial \phi} ;$$

This relation is exact for flows that are steady in the rotating frame and remains approximately valid for slowly varying structures (i.e., flow

time to a given heliocentric distance small compared to the scale of temporal variations at the source).

Equations (1) can be written in component form and manipulated into the pseudo-linear vector expression:

$$\frac{\partial \vec{U}}{\partial r} = \overline{\overline{F}} \cdot \frac{\partial \vec{U}}{\partial \theta} + \overline{\overline{H}} \cdot \frac{\partial \vec{U}}{\partial \phi} + \vec{G} \tag{2}$$

where $\vec{U}$ is a column vector composed of the dependent variables u_r, n, p, u_ϕ, and u_θ, $\overline{\overline{F}}$ and $\overline{\overline{H}}$ are nonlinear matrix coefficients, and $\vec{G}$ is a nonlinear five-vector driving term (the components of $\overline{\overline{F}}$, $\overline{\overline{H}}$, and $\vec{G}$ are listed in Appendix A). The characteristics are readily obtained from the eigenvalues of $\overline{\overline{H}}$ and $\overline{\overline{F}}$. We find three independent azimuthal characteristics

$$\lambda = \frac{\partial \theta}{\partial r} = \frac{V_\phi}{u_r\, r \sin\theta}, \qquad \frac{u_r V_\phi \pm c_s \sqrt{u_r^2 + V_\phi^2 - c_s^2}}{(u_r^2 - c_s^2)\, r \sin\theta} \tag{3a}$$

and three independent meridional characteristics

$$\epsilon = \frac{\partial \theta}{\partial r} = \frac{u_\theta}{r u_r}, \qquad \frac{u_r u_\theta \pm c_s \sqrt{u_r^2 + u_\theta^2 - c_s^2}}{r(u_r^2 - c_s^2)} \tag{3b}$$

where $V_\phi = u_\phi - \Omega r \sin\theta$

and $c_s^2 = \gamma \frac{p}{\rho}$.

The first value in each case is simply the streamline of the flow in the rotating frame, while the next two define the envelopes of pressure signals from a given point. We can guarantee that the quantities under the square root sign remain positive and the equations hyperbolic by situating our

inner boundary, r_o, outside the sonic critical point (at $\sim 35\ R_\odot$). The integration of equations (2) then reduces to a relatively tractable initial value problem in five unknowns.

NUMERICAL TECHNIQUES

Many numerical methods have been developed to cope with systems of coupled, hyperbolic partial differential equations such as (2). The explicit Eulerian approach described by MacCormack (1971) proves particularly efficient for multi-dimensional problems. Our implementation of the technique is inviscid, which means we must forgo any but the most rudimentary studies of shock formation. Thus the basic formulation cannot be applied to the distant solar wind, where shock structures dominate the flow (Gosling et al., 1976; Hundhausen and Gosling, 1976; Smith and Wolfe, 1976), nor to streams having sharp gradients near the sun and likely to steepen appreciable inside 1 AU. However, with some modification, it would be possible to add an explicit artificial viscosity and include the magnetic field in the model to permit consideration of these topics.

The tedious details of our numerical method are presented in Appendix A; here we will discuss only the broad outlines of the technique. The dependent variables $\vec{U} = (u_r, n, P, u_\phi, u_\theta)$ are specified on a fixed rectangular (θ, ϕ) mesh lying in the spherical surface, $r = r_o$, which constitutes the inner boundary. Figure 2 shows a schematic of the mesh superimposed on the heliocentric global coordinate system, with the azimuthal direction, ϕ, and the meridional direction (actually the colatitude), θ, defined as depicted. Note that the mesh covers only a portion of the surface, to minimize computer demands and to avoid numerical difficulties associated with the geometric singularities at the poles. Periodic boundary conditions are imposed at the azimuthal edge of the mesh, while the upper latitudinal boundary is a free surface,

with the meridional dervatives there being approximated by one-sided differences. This treatment is permissible provided we choose the boundary conditions such that the stream blends smoothly into uniform flow near and above the upper latitudinal edge of the mesh. As long as this edge lies only along the outermost fringes of the stream where the perturbations are very small, spurious effects upon the overall evolution are virtually nil. The lower latitudinal boundary is handled the same way, unless we are dealing with a stream that is symmetric about the equator. In that case, the lower half of the mesh may be dispensed with altogether, and the symmetry conditions simplify expression of the meridional dervatives.

Given $\vec{U}\ (r_o, \theta, \phi)$ everywhere on the mesh, we may advance the solution to $U\ (r_o + \Delta r, \theta, \phi)$ by our finite-difference form of equation (4). The magnitude of the Δr step is, for fixed $\Delta\theta$ and $\Delta\phi$, given by the Courant condition, which requires that the values at any given point be causally connected to the region demarcated by the upstream characteristics. The Courant step-size limit for this system is given by

$$\Delta r_c \leq \max\left(\frac{\Delta\phi}{\max|\lambda|}, \frac{\Delta\theta}{\max|\epsilon|}\right) \tag{4}$$

where λ and ϵ are the characteristic eigenvalues of equation (3). Should this condition be violated, spurious numerical instabilities arise which can quickly destroy the solution. This occurrence is easily avoided by updating the condition (4) every few integration steps and executing the computation at some prudent fraction of the specified limit, say, $0.8\ \Delta r_c$. In addition, it is necessary to check the accuracy

EXAMPLE - A VELOCITY-DRIVEN STREAM AT THE EQUATOR

To illustrate the fundamental processes involved in the 3-D stream interaction, we consider a simple model stream in which the radial velocity alone is a function of position at the inner boundary. In the real solar wind, we expect all flow quantities at the inner boundary to vary, leading to a rather complex evolution. These mixed-mode streams will be the subject of the next paper in this series. For this introductory study, however, it is imperative to work with basic, highly idealized structures to obtain a feel for the parameters most likely to be important in more realistic cases.

For our example, we have chosen a rather simple distribution of the radial velocity at the inner boundary, r_o. Since the source surface is a sphere centered on the sun, we represent this configuration by means of a contour plot projected onto a globe (Figure 3). (The projection is orthographic, meaning that the globe is viewed from infinity and free of parallax effects, though foreshortening remains.) North is at top, west at right--thus the contours are mapped onto the source surface ($r_o = 35\ R_\odot \approx .16$ AU) just as the sun appears in the sky. For reference, the usual global coordinates of latitude and longitude are provided with a 10^o spacing.

The contours of radial velocity in Figure 3 depict our highly idealized stream rising from a uniform surrounding slow flow of 290 km/sec to a peak velocity of 580 km/sec (marked by the "H") at the equator. The circular pattern and even spacing (Δ = 30 km/sec) of the contours indicates that the radial velocity variations are symmetric about the stream core. The overall width and amplitude of the distribution is

intended to mimic typical stream behavior near earth orbit (Gosling et al., 1972). (A slice through this distribution at constant θ is depicted in Figure 4. The variations in both θ and ϕ are of the form $[\sin(\pi x)/(\pi x)]^2$, where $|x| \leq 1$.) All the other variables--u_θ, u_ϕ, n, and p--are held constant on the source surface at the slow flow levels, which are adjusted to yield average solar wind conditions at 1 AU under the assumption of uniform radial adiabatic flow (Table I). For numerical convenience, the boundary conditions are periodic in ϕ. That is, another identical stream is located $\pm 120^\circ$ in azimuth from the one depicted. However, over the radial span of this calculation, the spacing of the streams suffices to guarantee that the interaction between them is negligible.

Our specification of the nonradial flow components at the inner boundary merits a brief digression here. These have been defined as equal to zero since it is our express intent to study the nonradial motions induced by the stream interaction. In fact, the neglect of motions which could conceivably be imposed as boundary conditions may be seen as only a minor handicap, since nonradial flows which are not driven by the dynamical interaction must decay as 1/r and thus should be unimportant relative to the large fluctuations that are generated by streams and grow with radius.

Figure 5 depicts the resultant contours of constant radial velocity, density, azimuthal velocity, and meridional velocity, respectively, at r = 1.0 AU. (Pressure and temperature are not shown, since the initial conditions and the use of the polytrope law requires n, T, and p all to be exactly in phase at all radii.) The Δ below each plot specifies the contour spacings, with highs and lows marked by "H" and "L". The symbol

η refers to the position of the original centerline of the pattern: thus, the central meridian of the source surface plot (Figure 3) is located 50^{o} to the right of the central meridian of the contours of Figure 5. This shift is due to solar rotation, as mentioned above.

In the u_r plot (Figure 5a) we have maintained the initial contour spacing of 30 km/sec to demonstrate the steepening that has occurred between r_o (Figure 2) and 1.0 AU. (The base level, of course, has risen because of the overall radial acceleration in the flow, as discussed in the mathematical section.) The high-velocity material at the core of the stream at r_o has overtaken the slower material to its right, resulting in the compression characterized by the compaction of the contours. Conversely, the wide spacing of the contours to the left denotes the rarefaction, where the fast plasma in the stream core has run away from the slower flow trailing the peak. Both the compression and rarefaction are clearly visible in the density contours (Figure 5b). (For reference, observe that the density far from the stream is about 7 cm^{-3}). The compression and the rarefaction are greatest at the equator because the initial amplitude of the stream maximizes there.

Figure 5(c,d) portrays the nonradial flow components at 1.0 AU. In the u_ϕ plot, the solid contours show flow to the right (the positive or corotating direction) while the dashed curves indicate motion to the left (the negative or anti-corotating direction). Similarly, in the u_θ plot solid contours depict positive (north-to-south) flow, while the dashed lines denote negative (south-to-north) motions. All of the behavior evident in Figure 5(c,d) is readily explained in terms of the pressure gradients generated by the θ-dependent stream interaction. Because the

stream interaction maximizes at the equator, the largest u_ϕ deflections and shears must occur there, also. However, just as the peak u_ϕ appears in the region of the largest azimuthal pressure gradients, so also must u_θ maximize along the steepest meridional gradients. Thus the peak u_θ motions are found well away from the equator and somewhat out of phase with u_ϕ. In addition, u_ϕ motions, being more directly driven by the stream interaction, develop larger amplitudes and sharper longitudinal variations than the u_θ flow. The relative amplitudes of and gradients in these two quantities may be adjudged by comparison of the contour spacings in Figure 5(c,d). (Bear in mind that the scale, Δ, differs by a factor of two in these two plots.)

Obtaining a clear mental picture of the flow patterns implied by Figure 5(c,d) requires a practiced eye. Therefore, in order to elucidate the relation of this flow to the overall geometry of the stream, we have prepared the velocity-vector plot, Figure 6. The relative magnitude and direction of the nonradial flow (corrected for projection effects) at a number of positions in the stream are indicated by the arrows. To set the scale, the small arrow beneath the globe has a value of 25 km/sec, while the large arrow measures 400 km/sec (the minimum radial velocity at 1 AU, for comparison purposes). The vectors have been superimposed on the density contours (equivalent to pressure contours in this velocity-driven case) of Figure 5b to emphasize the nonradial flow of material away from the compression and into the rarefaction, defining a weak global vortex motion. Similar large-scale vortices are also at work in the (r, ϕ) and (r, θ) planes, but their portrayal would be somewhat obscured by the relatively enormous magnitude of the radial velocity vector.

All the structure visible in Figures 5 and 6--the marked asymmetry in the radial velocity, the large-amplitude variations in the particle density, and the complex tangential vortex motions--all have been spawned in the mechanics of the stream interaction. The radial inflow of material into the high-density compression region as slow plasma is overtaken by fast leads to a nonradial outflow on a global scale, and vice versa for the rarefaction region.

The growth of this structure with radius is displayed graphically in Figure 7. There we view the fractional deviations

$$\frac{\Delta n}{n} = \left| \frac{n-n_o}{n_o} \right|, \quad \frac{\Delta u_\phi,\ \Delta u_\theta}{u_o} = \left| \frac{u_\phi,\ u_\theta}{u_o} \right|$$

of the density and nonradial flow components about n_o and u_o, the local slow-flow density and radial velocity, respectively. The curves in Figure 7 refer to the peak values anywhere in the stream; Δn and Δu_ϕ maximize at the equator in this case, whereas the greatest meridional deflection occurs at $\theta = 72^\circ$ near r_o, then gradually shifts toward the equator--lying at $\theta = 77^\circ$ at 1 AU--as the stream interaction develops. It is evident that while large variations in the density (and pressure) are generated as the stream steepens, the magnitude of the nonradial motions remains small, even out to 1.5 AU, where the appearance of numerical oscillations begins to affect the accuracy of the solution seriously. The growth in u_ϕ is tempered by two factors: first, since the interaction region lies approximately along the interplanetary spiral, the orientation of the associated pressure gradients systematically shifts to a more radial alignment as heliocentric distance increases; and, second, geometry

dictates that even if the angular scale, $\Delta\phi$, of the gradients is kept constant, the spatial scale, (r sin θ) $\Delta\phi$, must increase with r. Thus, in the absence of driving forces, conservation of angular momentum requires a decrease in the nonradial motion away from the sun, a fact we have exploited in setting u_ϕ and $u_\theta = 0$ at r_o.

Because the nonradial motions are driven by the pressure gradients built up in the stream interaction, u_θ is sensitive to the orientation of the interaction front relative to the meridional plane. In our example, the front is exactly perpendicular to the equator at $\theta = 90^\circ$; hence $u_\theta = 0$ there. The meridional motions that occur at higher latitudes are primarily edge flows, only marginally driven by the stream interaction. (In a subsequent paper, we will examine a case where the front is inclined to the equator, directly forcing material across the ecliptic plane.)

The lack of meridional flow at the equator does not mean that 3-D effects are negligible there. On the contrary, the vortex motion in Figure 6 implies a transport of mass, energy, and momentum away from the equator in the compression region and toward the equator throughout the rarefaction. These motions do not, in general, balance out. We compute the percentage mass-flux transport at a given latitude as:

$$M(\%) = \frac{M(r, \theta) - M(r_o, \theta)}{M(r_o, \theta)} \times 100 \qquad (8a)$$

where

$$M(r, \theta) = \int_\Phi d\phi \ (r^2 \rho u_r) \qquad (8b)$$

and Φ denotes summation across the entire stream at fixed θ.

In Figure 8 we plot this parameter as a function of θ at 1 AU. The greatest mass loss has been sustained at the equator and not at the latitudes where u_θ is greatest. Material has been systematically transported to higher latitudes by the equatorial divergence. This process proceeds monotonically with radius and approaches a value of 4.5% in the equatorial plane, at r = 1.5 AU, where it is gradually tapering off due to geometric effects.

The mass transport parameter M (%) primarily describes the action of meridional flow averaged over a span of longitude and is therefore global in nature. A more poignant measure of these effects on a local scale is presented in Figure 9. The three curves refer to the maximum absolute value (in arbitrary units) of the radial, azimuthal, and meridional divergence terms in the mass conservation equation, evaluated at the equator as a function of radius. Clearly, beyond about 0.75 AU, the nonradial terms rapidly diminish in relative importance, as the geometric decay overpowers the continual growth in u_ϕ and u_θ that accompanies the steepening of the stream. In addition, the meridional terms are relatively small compared to the azimuthal contributions as had been expected.

These two measures of nonradial effects--the longitudinally-averaged quantity M (%) and the locally-sensitive comparison of divergence terms--together suggest that while the equatorial portion of the stream continues to lose mass beyond 1 AU, this divergence must be rather diffuse and have little local effect upon the stream evolution except near the sun. That is, we conclude that the observable influence of the 3-D geometry upon the stream development at any fixed latitude is

largely confined to the region inside 0.75 AU and, furthermore, that the evolution is more strongly affected by the azimuthal motions than by the meridional motions. (The same arguments could have been applied to the momentum and energy divergence and transport terms; we have concentrated on the mass parameter because the nonradial effects are relatively largest in this quantity.)

An important implication of the above findings is that this stream does not spread very much in latitude in the supersonic flow regime of interplanetary space. Further support for this claim may be obtained by following the motion of tracer particles embedded in the flow. Figure 10a depicts an array of such markers uniformly dispersed across the source surface, r_o. (The initial spacing is $\Delta\theta = 2.0^o$, $\Delta\phi = 5.0^o$.) Differences in u_r as a function of position (see Figure 3) coupled with rotation lead, of course, to the dynamic stream interaction, which moves the particles about relative to one another. In Figure 10b we have tracked the markers to 1 AU, using the routine described in Appendix A. (This diagram has been rotated by the same angle η as the previous contour plots to facilitate comparison. The lines connect the particles in their original sequence at r_o.) We wish to make just two points: (1) the particles exhibit much greater relative displacement in ϕ that in θ, as predicted. And (2), one may mentally overlay the u_r and n contours of Figure 5 to relate pictorially the compression and rarefaction to the local density of the convected tracers. The displacement of the markers in θ is a straightforward process. However the ϕ-displacement of the markers has two components: one due to the actual u_ϕ motions seen in Figure 5c, and of a magnitude roughly comparable to the θ-displacement,

and a much larger one stemming from the rotational translation of the original $u_r(\phi)$ distribution. That is, the particles tied to the faster fluid elements near the stream core arrive at 1 AU relatively ahead (to the right) of the markers attached to the slower preceding material.

In the preceding paragraphs, we have investigated the dynamical processes associated with a fully nonlinear 3-D stream. It is instructive, therefore, to contrast the predictions of this model with those of familiar, less sophisticated formulations. To this end, we direct attention to the evolution of the stream in the immediate vicinity of the solar equator, where our 3-D solution predicts the maximum meridional transport effects. Figure 11 compares solutions for identical boundary conditions along the equator executed with nonlinear 3-D, 2-D, and 1-D models and with a 2-D linear model. Using this illustration, we will explore the effects attributable to the variation in geometrical properties among the models, and then we will consider the role of nonlinearities upon the dynamics.

Turning first to the dimensionality question, the 1-D solution (dashed) in Figure 11 refers to the so-called "(r, t)" model (Hundhausen, 1973), wherein only the radial terms in the equations (and, of course, rotation) are retained. The 2-D solution (light solid) goes one step further and takes the azimuthal motion into account (e.g., Goldstein, 1971), whereas our 3-D prediction (heavy solid) includes the full geometry. Figure 11 displays the radial velocity, density, and azimuthal velocity variations in the ecliptic plane at 1 AU for each of the three geometries. They are presented in time sequence form, with time increasing to the right in the usual manner of spacecraft data display.

However, we have chosen to employ the more fundamental heliocentric angular units rather than temporal units. For reference, the synodic angular velocity rate for an observer at 1 AU corresponds to 13.3° per day. Note also that time and azimuth, as defined in the spherical coordinate system attached to the sun, run in opposite directions. Hence, this time series is a mirror image of a slice through the equator of the distribution in Figure 5.

It is evident from Figure 11 that the 3-D geometry has had little influence on the evolution of the stream over that of the 2-D approximation. The real change comes in the transition from 2-D to 1-D (r, t) solutions. The azimuthal divergences have significantly broadened and reduced the compression at the leading edge by allowing material to slip laterally away from the interaction region; the 3-D case sees a further augmentation of this effect. The simplified geometry of the 1-D model leads to a gross overestimate of the dynamical reaction to the kinematic steepening of the stream and to the prediction of an exaggerated compression that is too steep and narrow. As a consequence, the 1-D radial velocity profile shows a stepped structure that portends shock-pair formation (actually occurring near 1.25 AU). The nonradial flow in the multi-dimensional models, on the other hand, relieves the stresses at the leading edge and thus delays the appearance of corotating shocks. (Due to numerical difficulties in this inviscid model, we cannot be more specific than to say that the multi-dimensional models do not shock before 1.5 AU.) We point out, however, that once the stream reaches 1 AU, Figure 9 suggests that the nonradial flow effects must wane, and

therefore the evolution at larger heliocentric distances must proceed in nearly 1-D fashion.

The essential nonlinearity of the stream interaction is demonstrated by comparison of the 2-D linear and nonlinear solutions found in Figure 11. The predictions of the linear model (dotted) were obtained by numerical integration of a 2-D formulation of the linear perturbation equations in (Siscoe and Finley, 1972), using the computational techniques described in this paper. The discrepancy between the linear and nonlinear models are even more striking than those between the 1-D and 2-D nonlinear solutions. The intrinsic inability of the linear model to steepen--due to the inadequate treatment of the crucial $(\vec{U}\cdot\nabla)\,\vec{U}$ term in the radial momentum equation--precludes its application to solar wind structures having large variations in the radial velocity (for more details, see Pizzo, 1977). On the other hand, a purely kinematic model--which may be viewed as the logical extreme of the 1-D nonlinear formulation--errs as disastrously in the opposite direction, through neglect of the dynamical reaction (i.e., pressure forces) of the system. (Calculations indicate that the kinematic model shocks near 0.8 AU for this example.)

These comparisons imply that accurate representation of solar wind dynamics inside 1.0 AU demands the use of models that are both multi-dimensional and nonlinear. While the nonradial flow may be small throughout the region of interest (e.g., refer to Figure 7), their cumulative effect in broadening the structure at the leading edge of the stream may be substantial. Apparently a 2-D nonlinear model may suffice for the study of many aspects of stream evolution; indeed, for some geometries and applications, the 3-D approach may prove extravagant.

However the 3-D model alone provides estimates of the meridional flow properties and further studies will be required to distinguish when the effects of meridional motions may be significant.

SUMMARY AND CONCLUSIONS

We have developed a numerical three-dimensional hydrodynamic model to study the effects of global, corotating stream evolution in interplanetary space. On a practical basis, the technique proves computationally efficient and is possessed of great versatility as well. With a minimum of effort, the model can be expanded to a 3-D MHD formulation or, alternatively, reduced in scope to 2-D and even 1-D descriptions. Indeed, the model may be applied to any corotating flow of astrophysical interest, so long as the governing partial differential equations are hyperbolic and well-behaved. With modest additional labor, shocks and discontinuities could be accommodated through the introduction of a suitable artificial viscosity.

The one simple stream model presented in this paper was selected to demonstrate the capabilities of our numerical techniques while also illustrating the basic phenomena to be encountered in corotating 3-D flows. A variety of graphical displays---the contour, velocity vector, and tracer particle plots--were utilized to elucidate the global aspects of the nonradial flow generated by the 3-D stream interaction. The primary finding is that the induced meridional motions are small, and so, therefore, are their effects upon the stream evolution. Thus much of the 3-D solar wind structure engendered in the upper reaches of the corona apparently persists in 1 AU and beyond, modified in transit by interplanetary processes that are essentially 2-D in nature.

Despite the hypothetical character of this example's boundary conditions, it is to be expected that the general sense of the results obtained should hold valid for a broad range of solar wind structures.

The flow is so heavily momentum-dominated that a significant departure from the traditional concepts of near-sun stream configurations--upon which the choice of this model was based--would be required before a substantial change in the dynamics of the situation could occur. Nevertheless, it would be inappropriate to generalize too freely upon the results of this one example, and, therefore, we defer such elaborations to the second paper in this series.

APPENDIX A - DETAILS OF NUMERICAL METHODS

I. Differencing Scheme and Matrices

We wish to numerically integrate the 3-D HD equations in matrix form:

$$\frac{\partial \vec{U}}{\partial r} = \overline{\overline{F}} \cdot \frac{\partial \vec{U}}{\partial \theta} + \overline{\overline{H}} \cdot \frac{\partial \vec{U}}{\partial \phi} + \vec{G} \tag{A.1}$$

where the independent variables are the usual (r, θ, ϕ) and the dependent variables are expressed as the vector

$$\vec{U} = \begin{pmatrix} U_r \\ n \\ P \\ U_\phi \\ U_\theta \end{pmatrix} .$$

Taking equations (1) in the order radial momentum, mass, polytrope, azimuthal momentum, and meridional momentum, the matrices $\overline{\overline{H}}$ and $\overline{\overline{F}}$ and the vector $\vec{G}$ are defined as

$$\overline{\overline{F}} = \frac{-1}{\alpha^2 r} \begin{pmatrix} U_\theta U_r & 0 & -U_\theta/\rho & 0 & -c_s^2 \\ -\rho U_\theta & \alpha^2 U_\theta/U_r & U_\theta/U_r & 0 & \rho U_r \\ -c_s^2 \rho U_\theta & 0 & U_\theta U_r & 0 & c_s^2 \rho U_r \\ 0 & 0 & 0 & \alpha^2 U_\theta/U_r & 0 \\ 0 & 0 & \alpha^2/\rho U_r & 0 & \alpha^2 U_\theta/U_r \end{pmatrix}$$

$$\bar{\bar{H}} = \frac{-1}{\alpha^2 r \sin\theta} \begin{pmatrix} V_\phi U_r & 0 & -V_\phi/\rho & -c_s^2 & 0 \\ -\rho V_\phi & \alpha^2 V_\phi/U_r & V_\phi/U_r & \rho U_r & 0 \\ -c_s^2 \rho V_\phi & 0 & V_\phi U_r & c_s^2 \rho U_r & 0 \\ 0 & 0 & \alpha^2/\rho U r & \alpha^2 V_\phi/U_r & 0 \\ 0 & 0 & 0 & 0 & \alpha^2 V_\phi/U_r \end{pmatrix}$$

and

$$\vec{G} = \frac{1}{\alpha^2} \begin{pmatrix} U_r C_1 - c_s^2 C_2/\rho \\ U_r C_2 - \rho C_1 \\ c_s^2 U_r C_2 - c_s^2 \rho C_1 \\ C_4/U_r \\ C_5/U_r \end{pmatrix}$$

where

$$\vec{C} = \frac{1}{r} \begin{pmatrix} U_\theta^2 + U_\phi^2 - \frac{GM_\theta}{r} \\ -2\rho U_r - \rho U_\theta \cot\theta \\ 0 \\ -U_\phi U_r - U_\phi U_\theta \cot\theta \\ U_\phi^2 \cot\theta - U_r U_\theta \end{pmatrix}$$

and

$$\alpha^2 = U_r^2 - c_s^2$$

$$c_s^2 = \gamma P/\rho$$

$$V_\phi = U_\phi - \Omega r \sin\theta \, .$$

In the supersonic region, equations (A.1) are everywhere hyperbolic, and the solution in the region ($r > r_o$) reduces to an initial-value problem. That is, we are given $\vec{U}$ over some span of θ and ϕ on the spherical surface r_o (see Figure 2) and are looking for a suitable numerical representation of equations (A.1) that will allow us to step the solution from r_o to $r + \Delta r$ and so on.

An efficient differencing scheme suggested by MacCormack (1971) and applied by Thomas et al. (1972), is a second-order, two-step, predictor-corrector of the form:

(step 1)

$$\tilde{U}_{ij}^{n+1} = U_{ij}^{n} + \Delta r \left[G_{ij} + F_{ij} \frac{U_{i,j+1}^{n} - U_{ij}^{n}}{\Delta\theta} + H_{ij} \frac{U_{i+1,j}^{n} - U_{ij}^{n}}{\Delta\phi} \right]$$

(step 2)

$$U_{ij}^{n+1} = \frac{1}{2} \left[U_{ij}^{n} + \tilde{U}_{ij}^{n+1} + \Delta r \left(\tilde{G}_{ij}^{n+1} + \tilde{F}_{ij}^{n+1} \frac{\tilde{U}_{ij}^{n+1} - \tilde{U}_{i,j-1}^{n+1}}{\Delta\theta} + \tilde{H}_{ij}^{n+1} \frac{\tilde{U}_{ij}^{n+1} - \tilde{U}_{i-1,j}^{n+1}}{\Delta\phi} \right) \right] \tag{A.2}$$

The superscript n refers to the radial mesh step, while subscript i and j refer to the azimuthal and meridional mesh nodes, respectively. The tilde denotes quantities computed from values generated in the first step; the vector and matrix symbols have been eliminated for clarity, but it is to be understood that (A.2) represents a matrix expression. This differencing scheme offers one particular advantage over dozens of other variants that could have been employed: storage is minimized since only U^n (and not G^n, H^n, F^n) need be retained from step 1 in order to execute step 2.

Additional savings in computer time can be realized by means of the coordinate transform found in Goldstein and Jokipii (1976). This transform is specifically tailored to the corotating stream problem and secures a larger radial step size by removing most of the azimuthal "motion" of the stream through the fixed mesh of the calculation. This apparent motion is nothing other than the spiral geometry of the interaction front. The transform effectively shifts the mesh to keep the mean spiral centered, and is almost equivalent to solving the system in the rotating frame.

The new independent variable in the azimuthal direction is

$$\xi = \phi + \Omega r/\bar{U}_r \qquad (A.3)$$

where Ω is the solar rotation rate and $\bar{U}_r$ some average radial velocity at r. When the transform is applied, the radial step-size criterion (4) is improved since

$$\lambda \to \lambda + \Omega/\bar{U}_r .$$

Note that the exact value of $\bar{U}_r$ is not critical; any rough average over the stream will serve the purpose, and, for greatest economy, need be updated only every few steps. One may keep track of the total absolute shift between the initial azimuthal coordinate system and the transformed system as

$$\Delta\phi = -\int_{r_o}^{r} \frac{\Omega}{\bar{U}_r(r)}\, dr$$

The differencing method (A.2) can, in principle, be used to solve any system of equations that can be cast in the form (A.1). Thus, using basically the same techniques, one can tackle a variety of models---from

1-D HD to 3-D MHD and even 2-D time-dependent MHD--merely by generating the appropriate expressions for $\bar{\bar{H}}$, $\bar{\bar{F}}$, and $\vec{G}$. The only requirement is that the solutions be hyperbolic everywhere within the region of interest and that they be well-behaved; i.e., not contain discontinuities or gradients that are too steep. This latter condition must remain somewhat ill-defined, but, in general, means that shocks are beyond the scope of the scheme described here. To be sure, (A.2) does contain a small amount of implicit artificial viscosity and therefore may tolerate weak discontinuities in some cases. However for situations of greater interest--say, the shock-dominated structures at several AU distance from the sun--the introduction of explicit artificial viscosity terms would be required (e.g., see Ch. 6 of Roache, 1972).

II. Accuracy Considerations

One of the simplest ways to test the accuracy of a numerical solution is to repeat the calculation using different values for the various mesh parameters. This may prove convergence to a limit, though not necessarily to the desired one. Another method is to substitute the generated solutions back into the original differential equations, a ploy that is useful in ferreting out local errors but insensitive to systematic deviations that become large cumulatively. Since equations (1) are not in explicit conservative form, we may resort to conservation laws to check our results. Easiest to implement is an integral summation of the conserved fluxes. If equations (1) are cast in conservative form and integrated in r and ϕ at fixed θ, then five relations--one for mass,

total energy, and each of the momentum fluxes--can be derived in the form

$$\int_{\Phi} d\phi \,[\text{flux density at } (r, \theta)] + \int_{R} dr \int_{\Phi} d\phi \left[\begin{array}{c}\text{change in flux density} \\ \text{at } \theta \text{ per unit radial} \\ \text{increment}\end{array}\right] = \text{const}$$

where the subscripts Φ and R denote integration over the entire azimuthal extent of the calculation from radius r_o to r. The kernel of the double integral contains a term arising from the exchange of momentum and energy among kinetic, thermal, and gravitational forms and a term related to the latitudinal transport contributed by the meridional motions. A sensitive measure of conservation on a local scale may be obtained through manipulation of equations (1). Along a streamline in the rotating frame, we find

$$P\rho^{-\gamma} = \text{const}$$

$$\frac{1}{2}\left(U_r^2 + U_\theta^2 + U_\phi^2\right) + \frac{\gamma}{\gamma-1}\frac{P}{\rho} - \frac{GM_\odot}{r} - \Omega r\, U_\phi \sin\theta = \text{const.}$$

The streamlines are specified by the first characteristic in equations (3) and are traced with the aid of a second-order Taylor expansion about the mesh nodes. The expressions are tedious and convolved, and their integration requires an iteration loop (see Pizzo, 1977).

These methods were used to evaluate the example presented in the text. For mesh resolutions $\Delta\Phi$ and $\Delta\phi$ of 2.5° and 1.0°, respectively, we find 1-2% overall conservation accuracy, with 5-8% local deviations in steep gradient regions, rapidly deteriorating near 1.5 AU where the evolution proceeds vigorously. (Note that more resolution is usually necessary in the azimuthal direction, as those gradients are

more directly driven by the stream interaction. Thus $\Delta\phi$ normally dictates the radial step criterion, Δr_c.) The computation time for this example, exclusive of graphics and diagnostic routines, was approximately two minutes on the GSFC IBM 360/91 computer.

ACKNOWLEDGMENTS

The bulk of this work was completed while the author was a graduate assistant at the High Altitude Observatory of the National Center for Atmospheric Research.* He expresses his gratitude to the entire HAO staff, and, in particular, to A. J. Hundhausen, T. E. Holzer, and R. G. Athay. In addition, he is deeply indebted to J. M. Malville, S. T. Suess, J. T. Gosling, J. Feynman, and L. Burlaga for their continued support over the years. The referees' comments were of great assistance in revising this paper.

*The National Center for Atmospheric Research is funded by the National Science Foundation.

REFERENCES

Barouch, E., and L. F. Burlaga, Three-dimensional interplanetary stream magnetism and energetic particle motion, J. Geophys. Res., 81, 2103, 1976.

Dobrowolny, M. and G. Moreno, Latitudinal structure of the solar wind and interplanetary magnetic field, Space Sci. Rev., 18, 685, 1976.

Dryer, M. and R. S. Steinolfson, MHD solution of interplanetary disturbances generated by simulated velocity perturbations, J. Geophys. Res., 81, 5413, 1976.

Goldstein, B. E. Nonlinear corotating solar wind structure, CSR-P-71-63, Mass. Inst. of Tech., 1971.

Goldstein, B. E., and J. R. Jokipii, Effects of stream-associated fluctuations upon the radial evolution of average solar wind parameters, J. Geophys. Res., 82, 1095, 1977.

Gosling, J. T., A. J. Hundhausen, V. Pizzo, and J. R. Asbridge, Compressions and rarefactions in the solar wind: Vela 3, J. Geophys. Res., 77, 5442, 1972.

Gosling, J. T., A. J. Hundhausen, and S. J. Bame, Solar wind stream evolution at large heliocentric distances: Experimental demonstration and the test of a model, J. Geophys. Res., 81, 2111, 1976.

Gosling, J. T., J. R. Asbridge, S. J. Bame, and W. C. Feldman, Solar wind stream interfaces, J. Geophys. Res., 83, 1401, 1978.

Hundhausen, A. J., Nonlinear model of high-speed solar wind streams, J. Geophys. Res., 78, 1528, 1973.

Hundhausen, A. J., An interplanetary view of coronal holes, A Monograph on Coronal Holes, Ch. 7, (J. B. Zirker, ed.) Univ. of Colo., 1977.

Hundhausen, A. J. and J. T. Gosling, Solar wind structure at large heliocentric distances: An interpretation of Pioneer 10 observations, J. Geophys. Res., 81, 1436, 1976.

MacCormack, R. W. Numerical solution of the interaction of a shock wave with a laminar boundary layer, Proc. of the Second Intl. Conf. on Numerical Methods in Fluid Dyn., (M. Holt, ed.), Lecture Notes in Physics, vol. 8, Springer-Verlag, N. Y., p. 151, 1971.

Matsuda, T., and T. Sakurai, Dynamics of the azimuthally-dependent solar wind, Cosmic Electrodyn., 3, 97, 1972.

Nakagawa, Y., and R. E. Wellck, Numerical studies of azimuthal modulations of the solar wind with magnetic fields, Solar Phys., 32, 257, 1973.

Nerney, S. F. and S. T. Suess, Restricted three-dimensional stellar wind modeling, Astrophys. J., 196, 837, 1975.

Parker, E. N., Dynamics of the interplanetary gas and magnetic fields, Astrophys. J., 128, 664, 1958.

Pizzo, V., A three-dimensional model of high-speed streams in the solar wind, Ph. D. thesis, Univ. of Colo., Boulder, CO, 1977.

Pizzo, V. and L. Burlaga, The dynamics of steep stream configurations near the sun, EOS, 58, 1225, 1977 (abstract only).

Roache, P. J., Computational Fluid Dynamics, Hermosa Publ., Albuquerque, NM, 1972.

Rosenbauer, H., R. Schwenn, E. Marsch, B. Meyer, H. Miggenrieder, M. D. Montgomery, K. H. Muhlhauser, W. Pilipp, W. Voges, and S. M. Zink, A survey of initial results of the Helios plasma experiment, J. Geophys. Res., 42, 561, 1977.

Siscoe, G. L. and L. T. Finley, Meridional (north-south) motions of the solar wind, Solar Phys., 9, 452, 1969.

Siscoe, G. L. and L. T. Finley, Solar wind structure determined by corotating coronal inhomogeneities, 2, arbitrary perturbations, J. Geophys. Res., 77, 35, 1972.

Smith, E. J. and J. H. Wolfe, Observations of interaction regions and corotating shocks between one and five AU: Pioneers 10 and 11, Geophys. Res. Lett., 3, 137, 1976.

Suess, S. T., Three-dimensional solar wind, J. Geophys. Res., 77, 567, 1972.

Suess, S. T., A. J. Hundhausen, and V. Pizzo, Latitude-dependent nonlinear high-speed solar wind streams, J. Geophys. Res., 80, 2023, 1975.

Thomas, P. D., M. Vinokur, R. A. Bastianon, and R. J. Conti, Numerical solution for three-dimensional inviscid supersonic flow, AIAA Journal, 10, 887, 1972.

TABLE I

PHYSICAL PARAMETERS FOR THE SLOW FLOW

	$r_o = 35\ R_\odot$	$r = 1.0$ AU
u_r (km/sec)	290	401
n (cm^{-3})	370	7.1
T (^oK)	1.12×10^6	8.0×10^4
u_ϕ (km/sec)	0	0
u_θ (km/sec)	0	0

FIGURE CAPTIONS

Figure 1 Schematic of the stream interaction in the inertial frame. The view is from above the north pole of the sun, looking down on the ecliptic plane. Spatial differences in the nearly radial expansion (indicated by the dark vectors) couple with solar rotation to produce compressions (shaded) and rarefactions in the interplanetary medium. Secondary nonradial motions are driven by pressure gradients built up in the stream interaction (large open arrows). Magnetic field lines--which correspond to streamlines of flow in the rotating frame--are drawn out into the spiral configuration as shown.

Figure 2 Definition of coordinate system and mesh parameters at fixed radius. The computational mesh (dark grid pattern) covers only a portion of the total spherical surface.

Figure 3 Boundary conditions for the example in the text. The contours of constant radial velocity are spaced at an interval, Δ, of 30 km/sec.

Figure 4 Longitudinal slice through the distribution of Figure 3. The curve is depicted as a time sequence increasing to the right (the usual observational convention), while azimuth increases to the left.

Figure 5 Contours of constant radial velocity (a), number density (b), azimuthal velocity (c), and meridional velocity (d), for the stream at 1.0 AU. The solid contours in (c) refer to westward (positive or corotating) flow, the dashed contours to eastward (negative or anti-corotating) flow. The solid contours in (d) refer to southward (positive) flow, the dashed contours to northward (negative flow. The peak values are denoted by the "H", the minima by "L", and the contour intervals by Δ. The contours have been shifted in longitude by the angle η from the original centerline to account for rotation (see text).

Figure 6 Nonradial flow vectors at 1.0 AU, superimposed on the density contours of Figure 6(b). The scale is set by the vectors at bottom.

Figure 7 Growth of density and nonradial velocity perturbations with radius. The curves refer to the peak values anywhere within the stream.

Figure 8 Net percentage mass-flux transport as a function of colatitude, θ, at 1.0 AU. Material has been moved away from the equator toward higher latitudes by the meridional flow.

Figure 9 Radial dependence (at the equator) of the peak values of radial, azimuthal, and meridional divergence terms in the mass conservation equation.

Figure 10 Relative displacement of tracer particles imbedded in flow between r_o and 1.0 AU. The arrow identifies the series of particles lying along the central meridian at r_o. Through interpolation, one may map the interplanetary distortions of any pattern (e.g., magnetic topology in weak-field limit) frozen to the flow.

Figure 11 Comparison of stream models in equatorial plane. Predictions of radial velocity, density, and azimuthal velocity at 1.0 AU are presented for 3-D, 2-D, and 1-D nonlinear, and 2-D linear formulations.

STREAM INTERACTION SCHEMATIC
(INERTIAL FRAME)

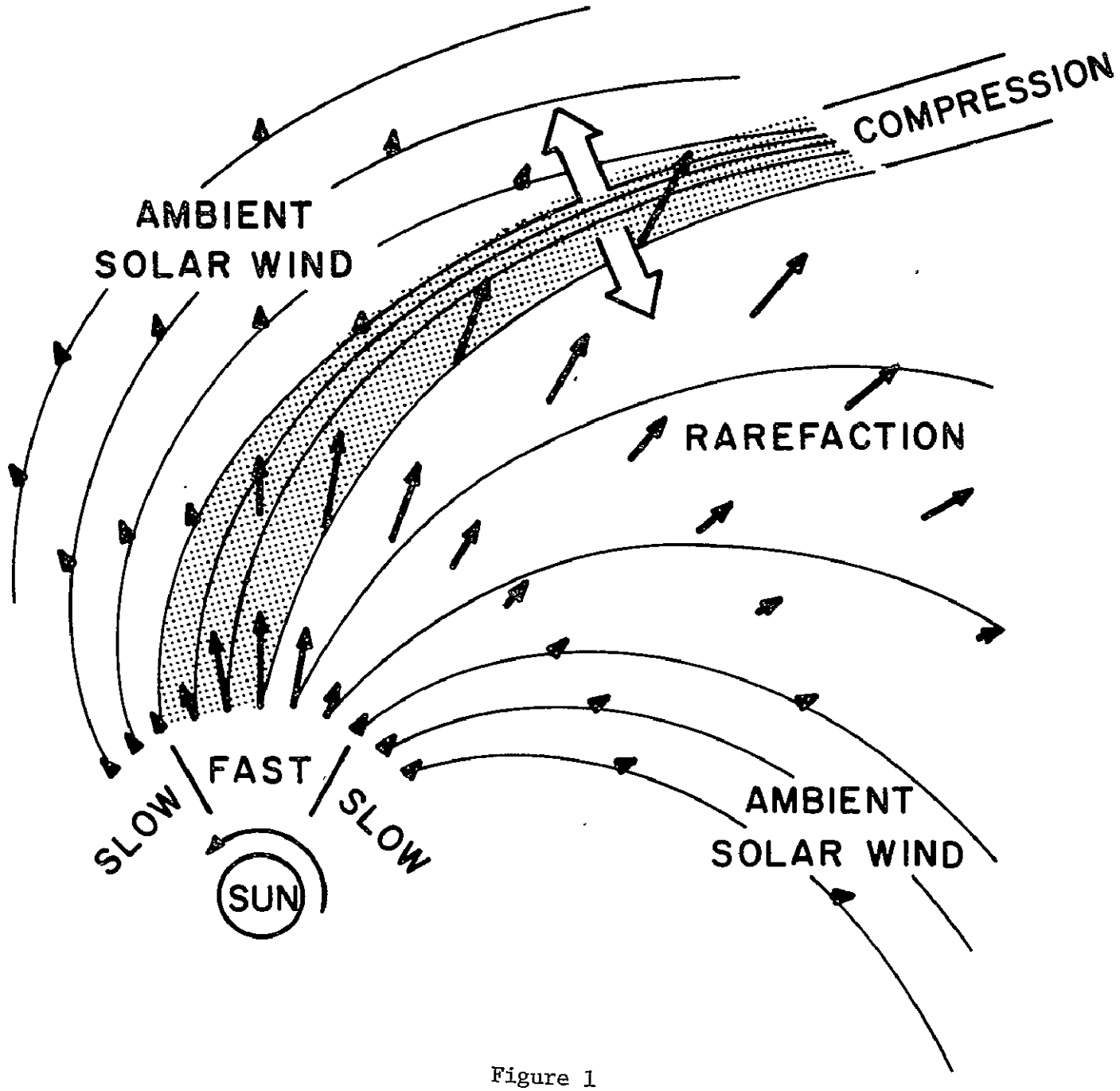

Figure 1

SCHEMATIC OF MESH

DEFINITION OF PARAMETERS AT CONSTANT RADIUS

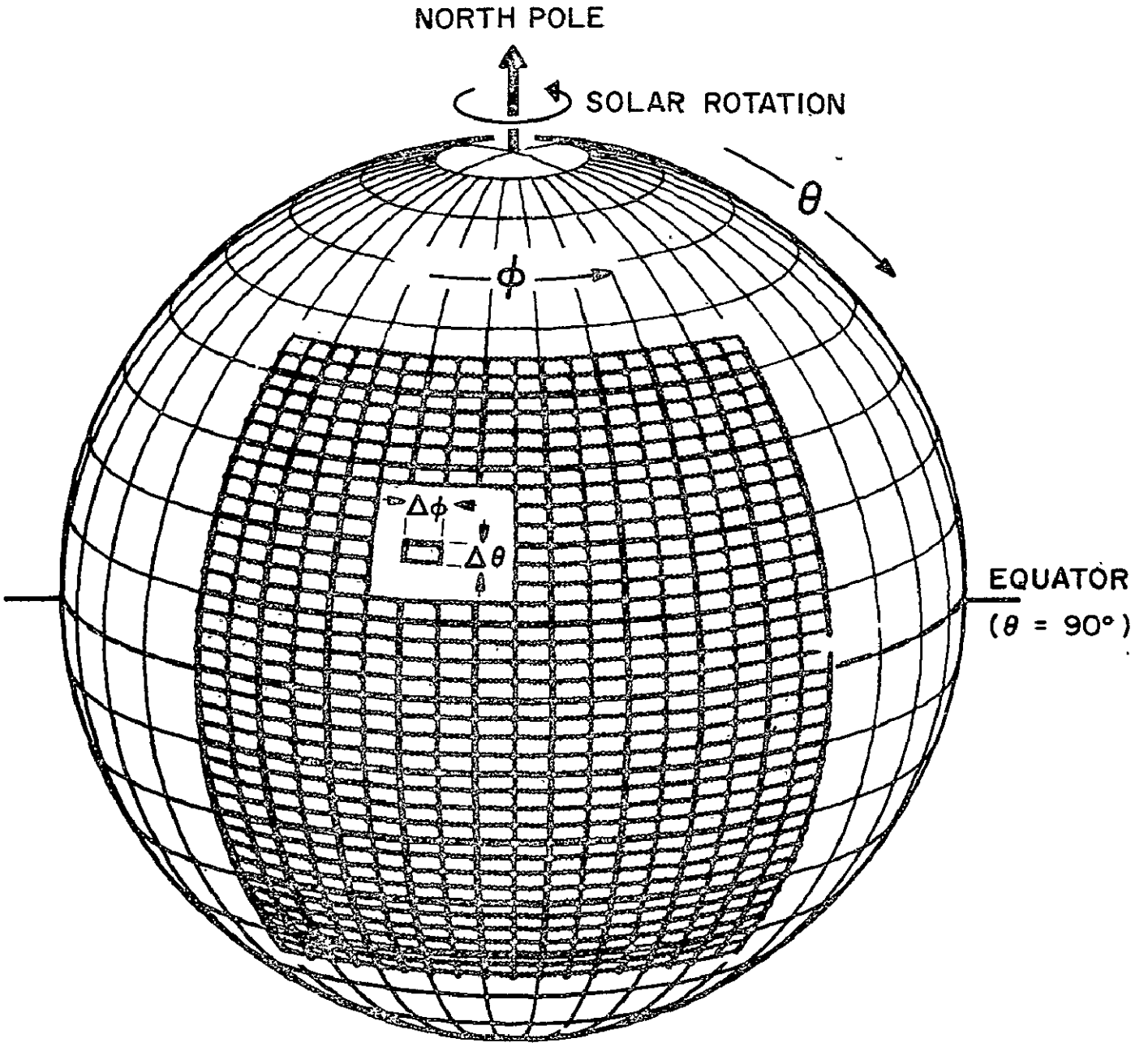

Figure 2

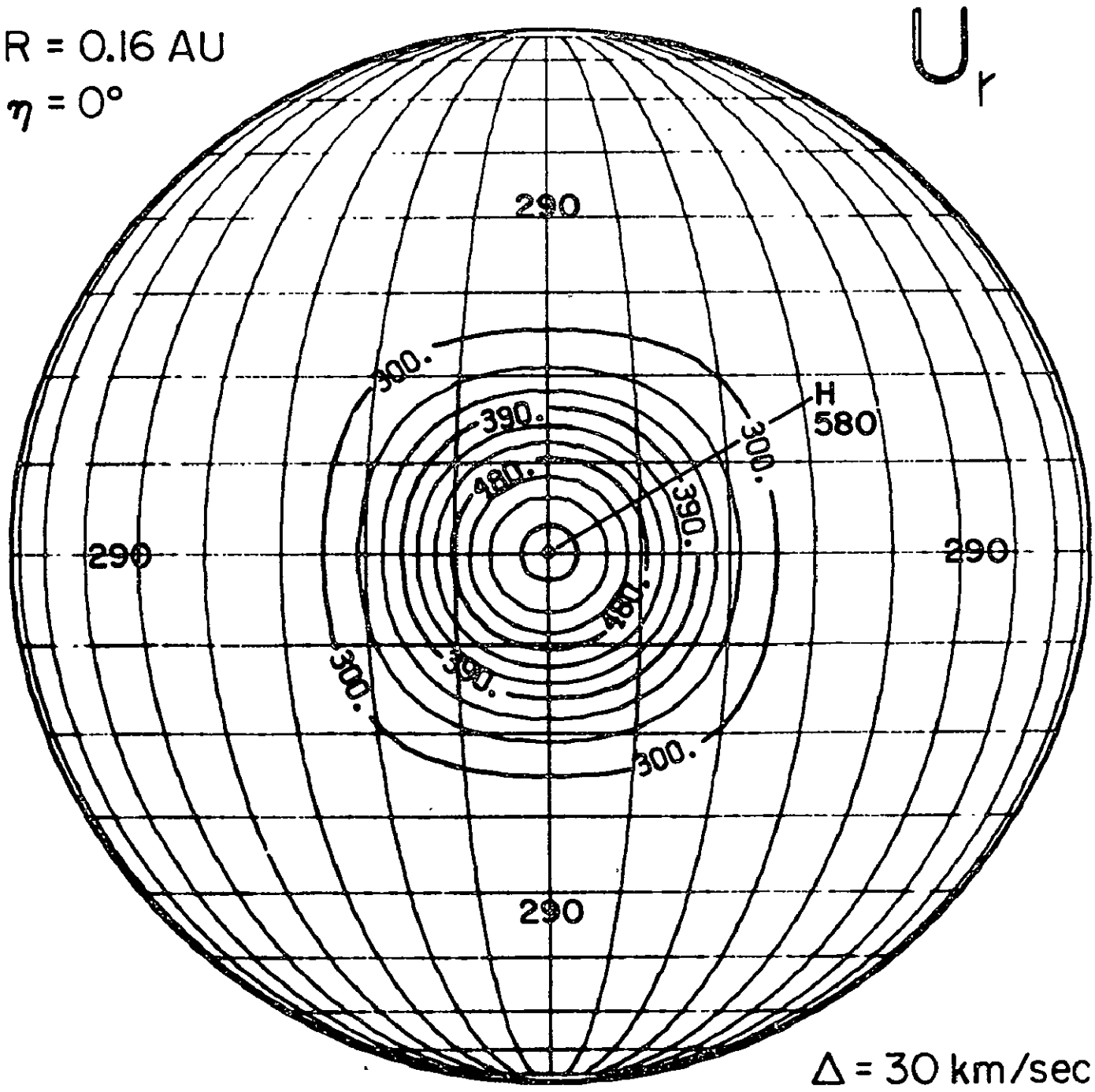

Figure 3

INPUT STREAM PROFILE

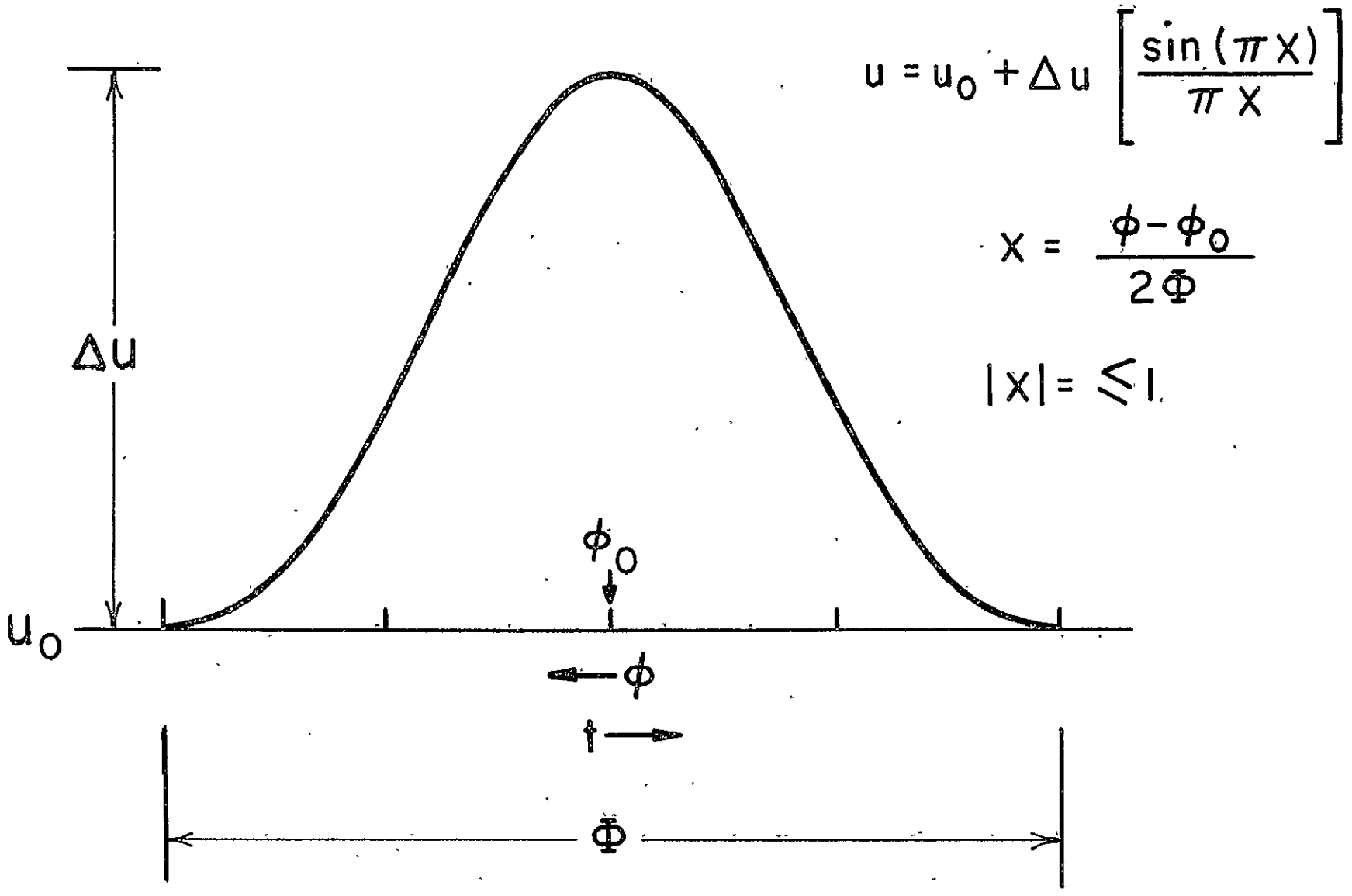

Figure 4

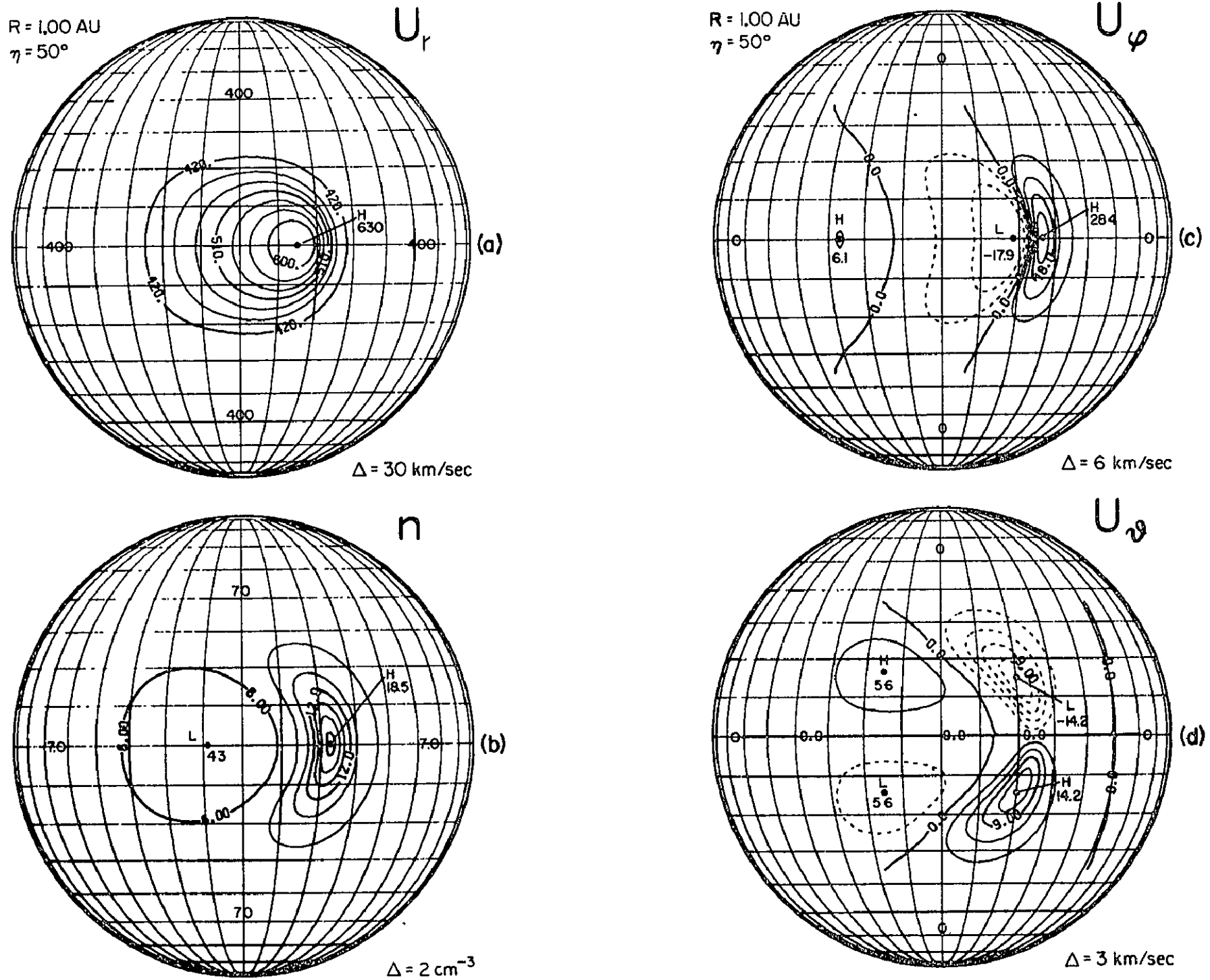
R = 1.00 AU
η = 50°
U_r
400
420.
H
630
600.
510.
(a)
Δ = 30 km/sec
R = 1.00 AU
η = 50°
U_φ
H
6.1
L
-17.9
H
28.4
(c)
Δ = 6 km/sec
n
70
H
18.5
L
43
7.0
(b)
Δ = 2 cm⁻³
U_ϑ
H
5.6
L
-14.2
L
5.6
H
14.2
(d)
Δ = 3 km/sec

Figure 5

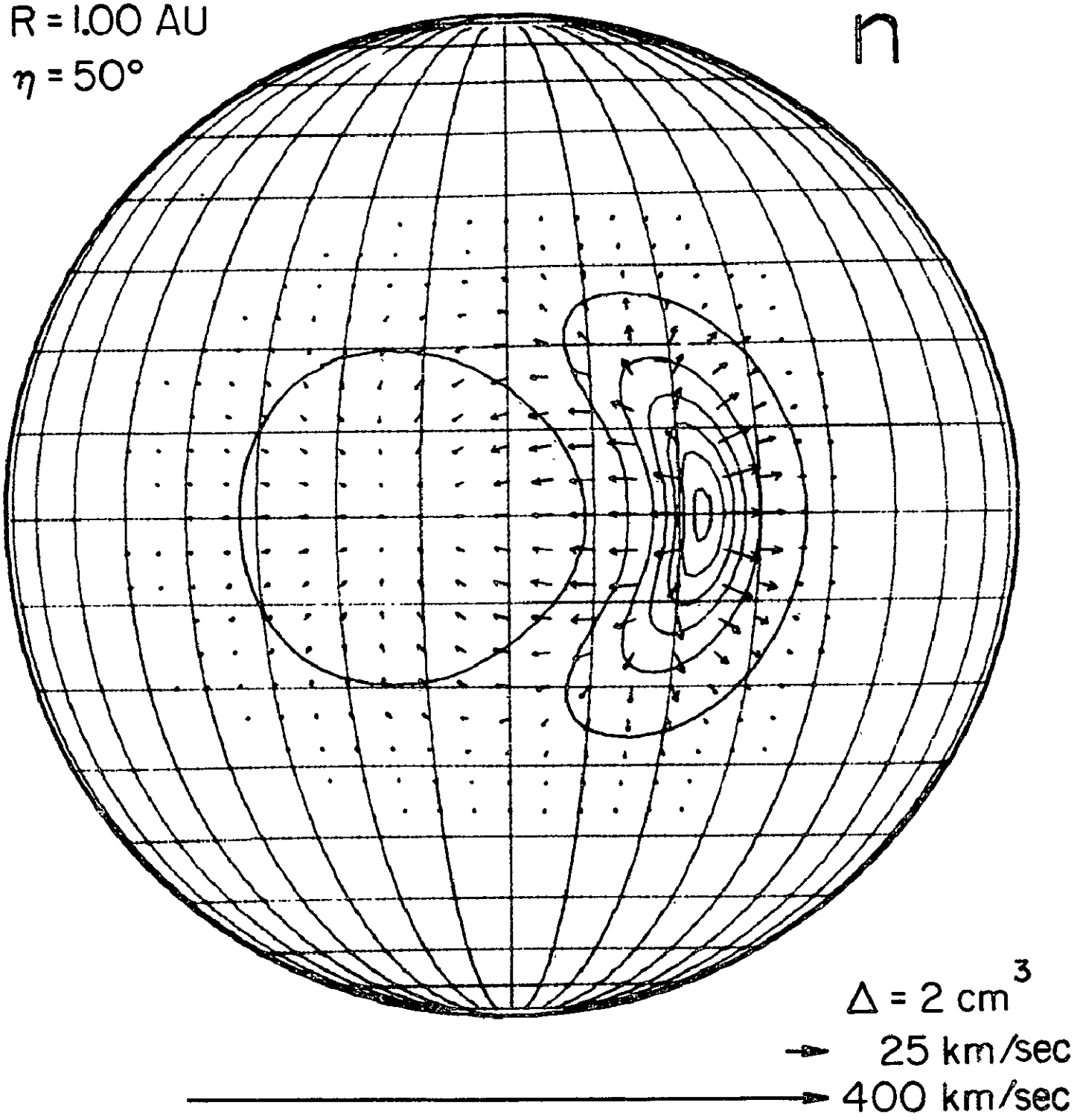

Figure 6

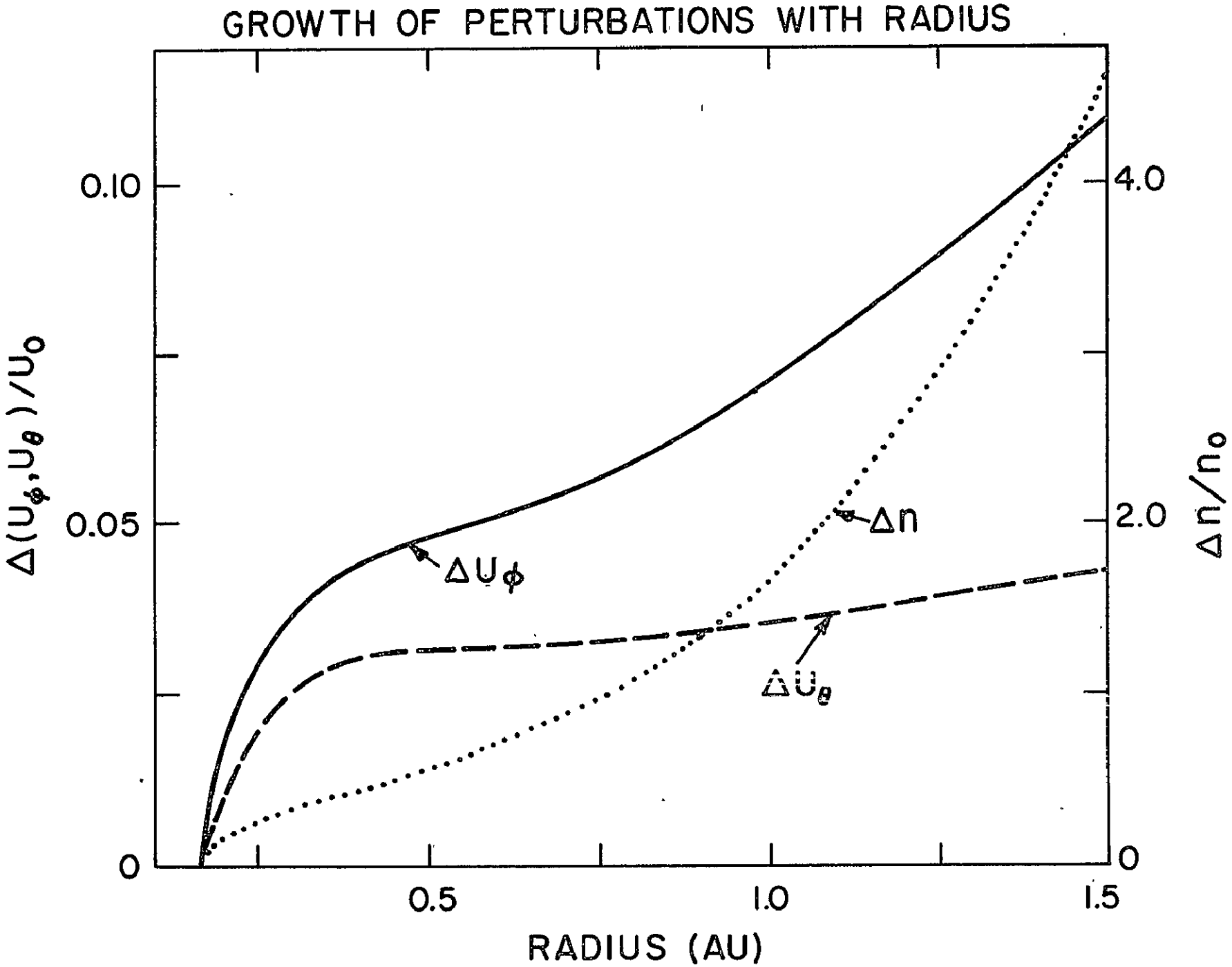
GROWTH OF PERTURBATIONS WITH RADIUS
0.10
0.05
0
4.0
2.0
0
0.5
1.0
1.5
RADIUS (AU)
Δ(Uφ, Uθ)/U0
Δn/n0
ΔUφ
Δn
ΔUθ

Figure 7

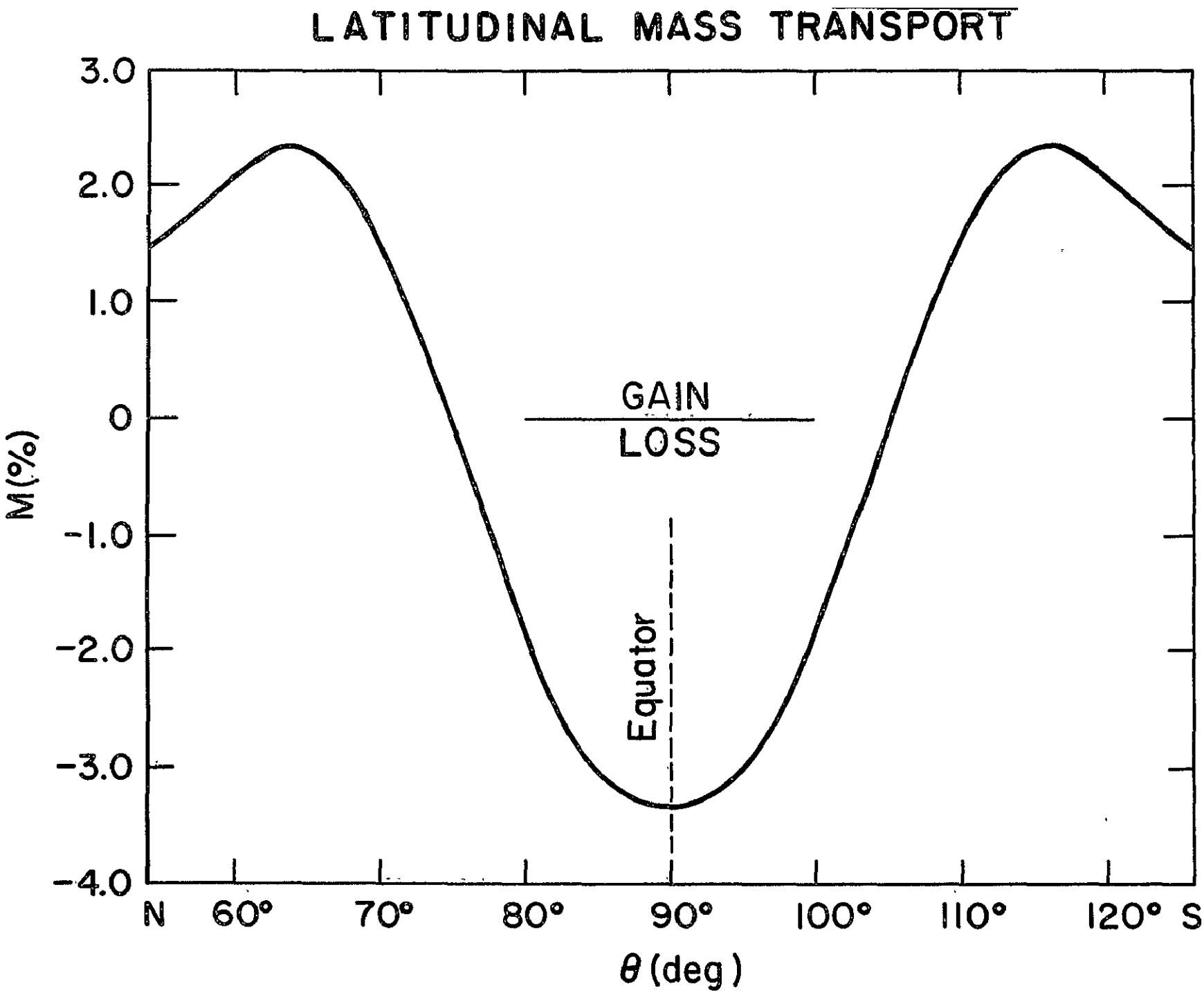
LATITUDINAL MASS TRANSPORT
3.0
2.0
1.0
0
-1.0
-2.0
-3.0
-4.0
M(%)
GAIN
LOSS
Equator
N
60°
70°
80°
90°
100°
110°
120°
S
θ (deg)

Figure 8

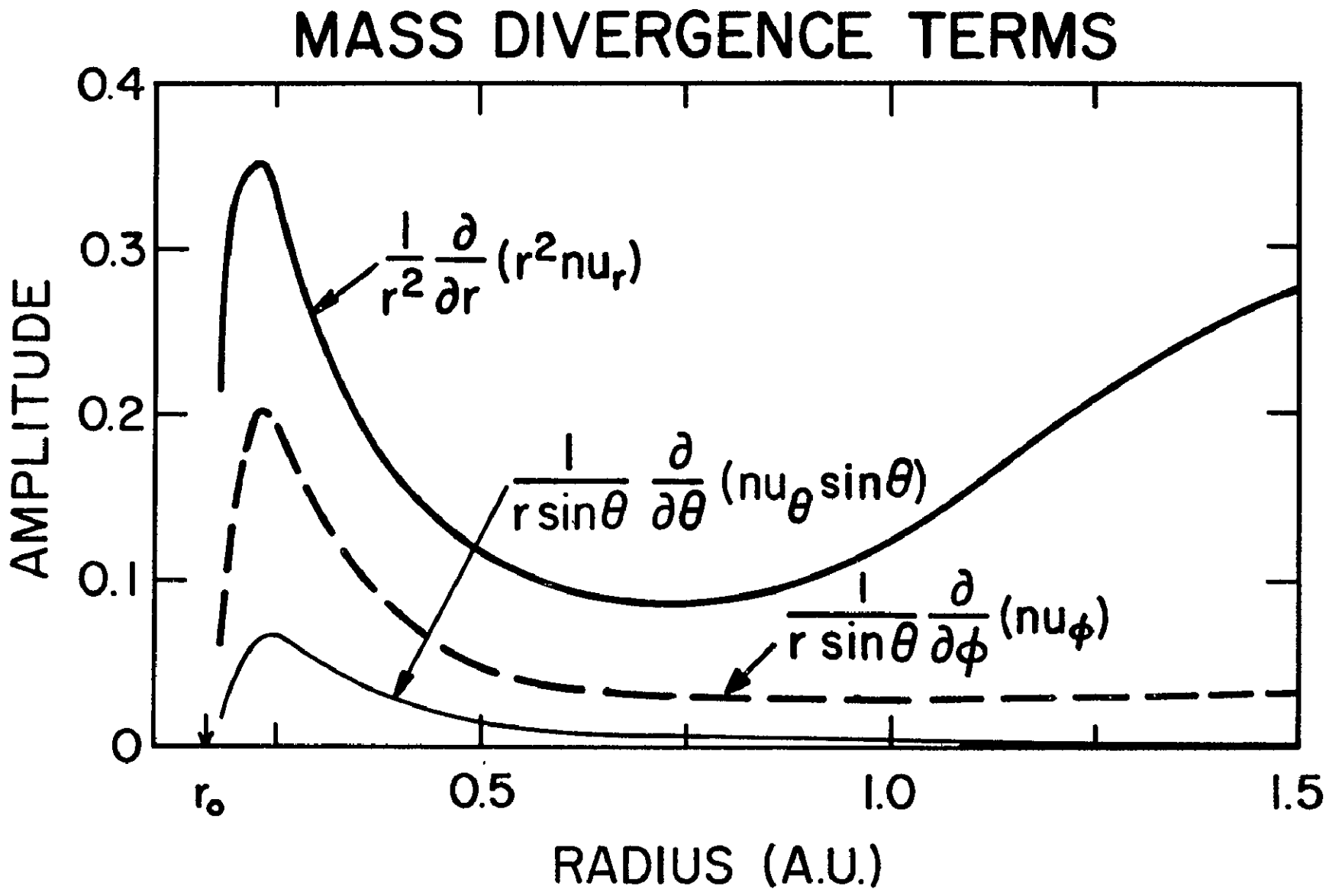
MASS DIVERGENCE TERMS
AMPLITUDE
0.4
0.3
0.2
0.1
0
$\frac{1}{r^2}\frac{\partial}{\partial r}(r^2 nu_r)$
$\frac{1}{r\sin\theta}\frac{\partial}{\partial\theta}(nu_\theta \sin\theta)$
$\frac{1}{r\sin\theta}\frac{\partial}{\partial\phi}(nu_\phi)$
r_o
0.5
1.0
1.5
RADIUS (A.U.)

Figure 9

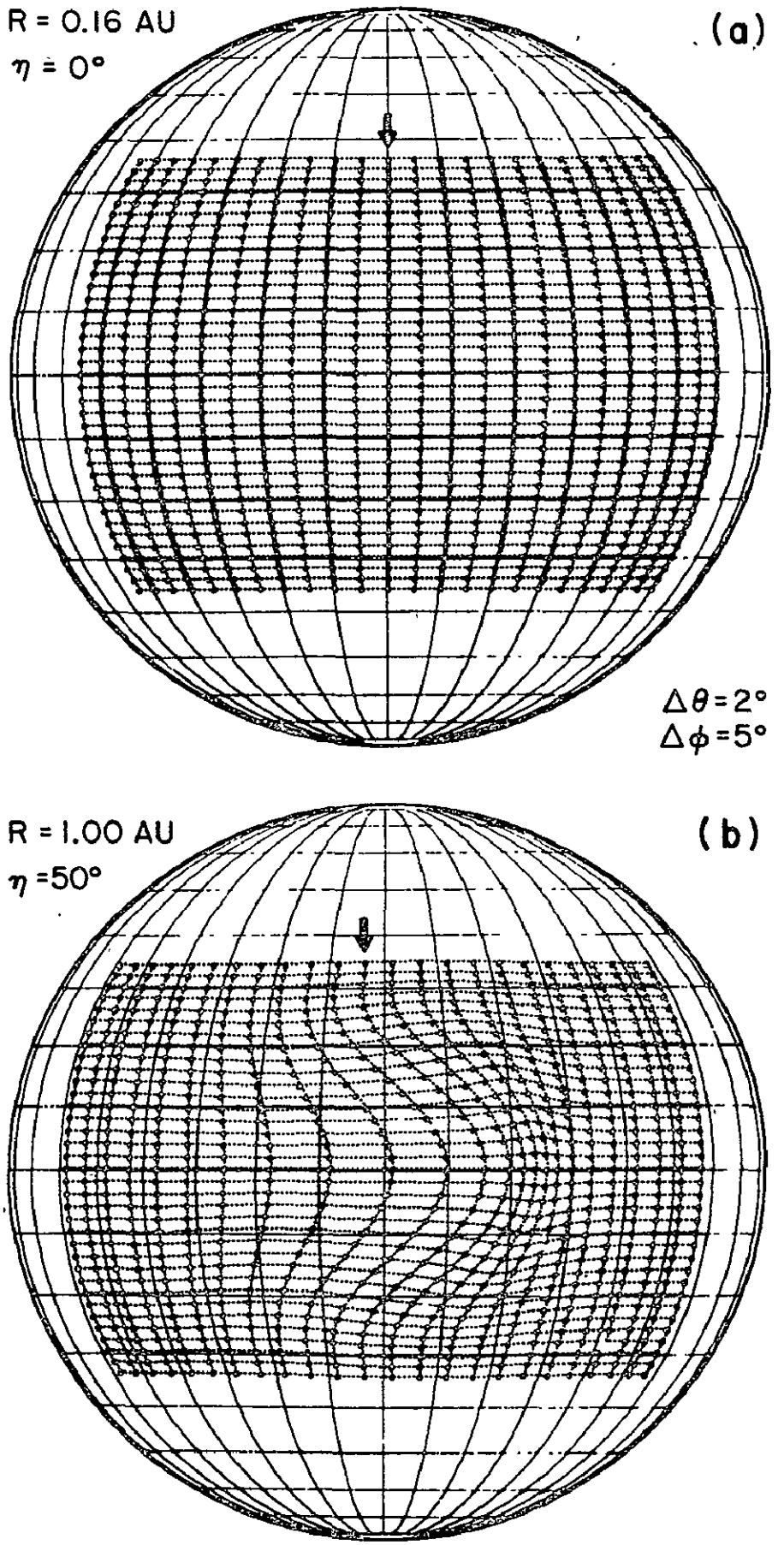

Figure 10

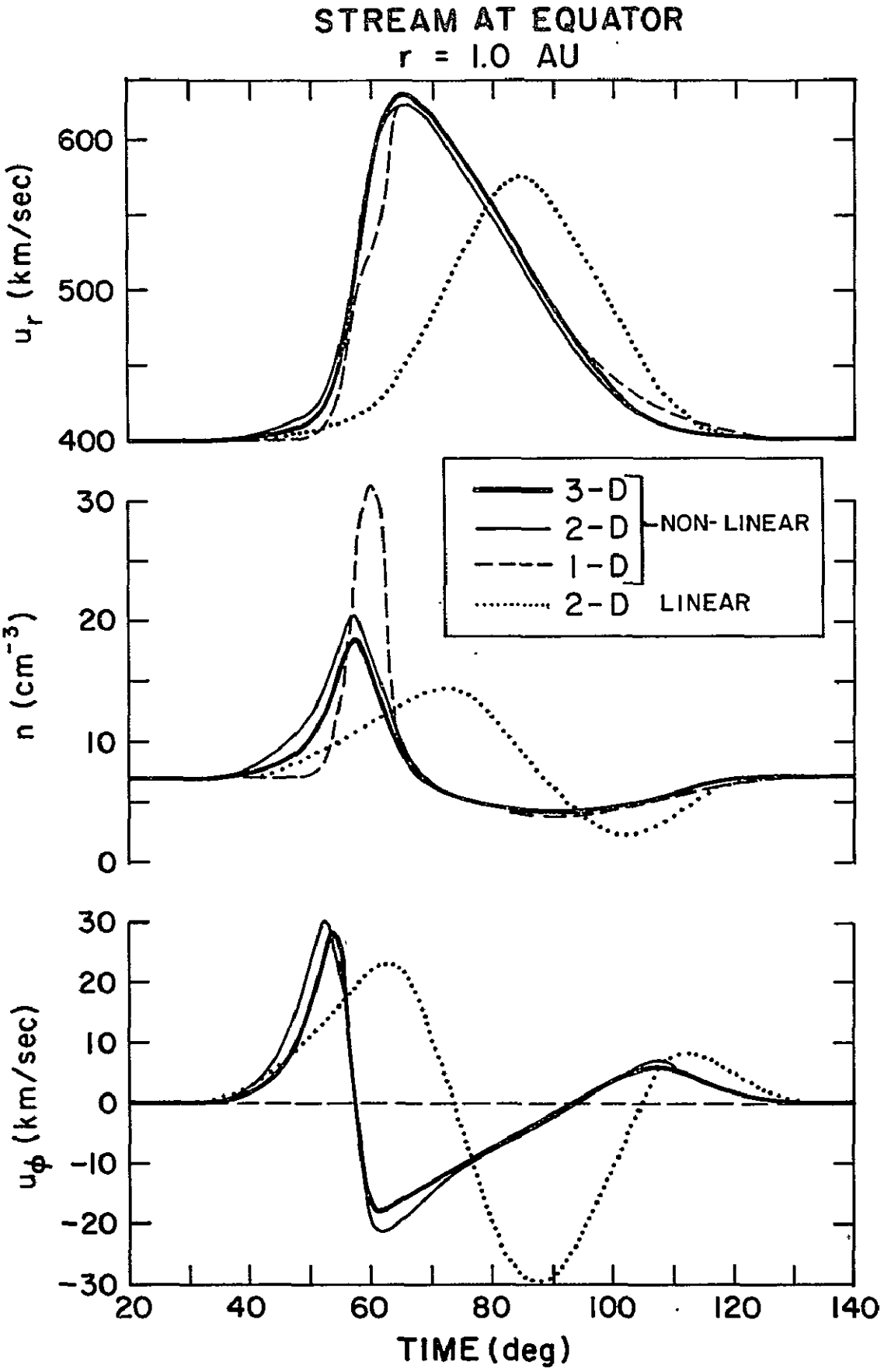
STREAM AT EQUATOR
r = 1.0 AU
u_r (km/sec)
600
500
400
n (cm^{-3})
30
20
10
0
3-D
2-D
1-D
NON-LINEAR
2-D LINEAR
u_ϕ (km/sec)
30
20
10
0
-10
-20
-30
20
40
60
80
100
120
140
TIME (deg)

Figure 11

1. Report No.	2. Government Accession No.	3. Recipient's Catalog No.
TM 79580		

4. Title and Subtitle	5. Report Date
A Three-Dimensional Model of Corotating Streams in the Solar Wind I. Theoretical Foundations	June 1978
	6. Performing Organization Code
7. Author(s) Victor J. Pizzo (NAS/NRC Resident Research Associate)	8. Performing Organization Report No.
9. Performing Organization Name and Address NASA/GSFC Laboratory for Extraterrestrial Physics Interplanetary Physics Branch, Code 692 Greenbelt, MD 20771	10. Work Unit No.
	11. Contract or Grant No.
	13. Type of Report and Period Covered Technical Memorandum
12. Sponsoring Agency Name and Address	14. Sponsoring Agency Code

15. Supplementary Notes

16. Abstract This paper is concerned with the development of the theoretical and mathematical background pertinent to the study of steady, corotating solar wind structure in all three spatial dimensions (3-D). The dynamical evolution of the plasma in interplanetary space (defined as the region beyond roughly 35 $R_\odot$ where the flow is supersonic) is approximately described by the nonlinear, single-fluid, polytropic (magneto-) hydrodynamic equations. We outline efficient numerical techniques for solving this complex system of coupled, hyperbolic partial differential equations. The present formulation is inviscid and non-magnetic, but our methods allow for the potential inclusion of both features with only modest modifications. We examine one simple, highly idealized, hydrodynamic model stream to illustrate the fundamental processes involved in the 3-D dynamics of stream evolution. We find that spatial variations in the rotational stream interaction mechanism produce small nonradial flows on a global scale that lead to the transport of mass, energy, and momentum away from regions of relative compression and into regions of relative rarefaction. The magnitude of this transport is small, but inside 1 AU the nonradial flow can significantly retard shock formation by allowing fluid in the compressions to slip laterally, thereby partially relieving the stresses built up in the stream interaction. Comparison with simpler models demonstrates the essential nonlinear, multi-dimensional nature

17. Key Words (Selected by Author(s))	18. Distribution Statement
Stream model, three-dimensions, hydrodynamic, nonlinear	

19. Security Classif. (of this report)	20. Security Classif. (of this page)	21. No. of Pages	22. Price*
U	U	52	

*For sale by the National Technical Information Service, Springfield, Virginia 22151.

16. Abstract Cont'd.

of the interplanetary dynamics. A subsequent paper will be devoted to the investigation of a wide range of more realistic model streams.